

Supporting Information

Ni(II) 10-Phosphacorrole: A Porphyrin Analogue Containing Phosphorus at the *Meso* Position

Hiroto Omori,[†] Satoru Hiroto,[†] Youhei Takeda,[‡] Heike Fliegl,^{§*} Satoshi
Minakata,[‡] and Hiroshi Shinokubo^{†*}

[†]Department of Molecular and Macromolecular Chemistry, Graduate School of Engineering, Nagoya University, Furo-cho, Chikusa-ku, Nagoya, Aichi 464-8603, Japan.

[‡]Department of Applied Chemistry, Graduate School of Engineering, Osaka University, Yamadaoka 2-1, Suita, Osaka 565-0871, Japan

[§]Karlsruhe Institute of Technology, Institute of Nanotechnology, Hermann-von-Helmholtz-Platz 1, 76344 Eggenstein-Leopoldshafen, Germany

E-mail: hshino@chembio.nagoya-u.ac.jp; heike.fliegl@kit.edu

Table of Contents

Instrumentation and Materials	S2
Synthesis and Compound Data	S2
NMR Spectra of Compounds	S4
X-Ray Diffraction Analysis	S11
Electrochemical Analysis	S17
Theoretical Calculations	S18
GIMIC Calculation	S25

Instrumentation and Materials

¹H NMR (500 MHz), ¹³C NMR (126 MHz), and ³¹P NMR (202 MHz) spectra were recorded on a Bruker AVANCE III HD spectrometer, and chemical shifts were reported as the delta scale in ppm relative to CHCl₃ ($\delta = 7.26$ ppm) and CH₂Cl₂ ($\delta = 5.31$ ppm) for ¹H NMR and CDCl₃ ($\delta = 77.16$ ppm) for ¹³C NMR, and H₃PO₄ ($\delta = 0.00$ ppm) for ³¹P NMR. UV/vis/NIR absorption spectra were recorded on a Shimadzu UV-2550 or JASCO V670 spectrometer. High-resolution mass spectra were recorded on a Bruker microTOF using positive mode ESI-TOF method for acetonitrile solutions. Unless otherwise noted, materials obtained from commercial suppliers were used without further purification.

Synthesis and Compound Data

P-Mesityl-*meso*-mesityl-10-phosphacorrole **2**.

A Schlenk tube containing bis(α,α' -dibromodipyrrin) Ni^{II} complex **1**¹ (179 mg, 200 μ mol), *t*-BuOK (134 mg, 1.20 mmol), and PdCl₂(dppf)•CH₂Cl₂ (49.1 mg, 60.1 μ mol) was evacuated and then refilled with N₂. To the tube, dry and degassed toluene (10.0 mL) and mesitylphosphine (324 mg, 2.13 mmol) were added. The mixture was stirred at 90 °C for 15 h. The reaction mixture was extracted with CH₂Cl₂. The organic layer was washed with water, dried over anhydrous Na₂SO₄, and concentrated in vacuo. Purification by silica-gel column chromatography with CH₂Cl₂/hexane afforded the title compound in 52% (75.1 mg, 103 μ mol) as a brown solid. ¹H NMR (CDCl₃): δ 7.69 (d, $J = 4.0$ Hz, 2H, pyrrole- β), 7.60 (d, $J = 4.0$ Hz, 2H, pyrrole- β), 7.40 (d, $J = 4.0$ Hz, 2H, pyrrole- β), 7.35–7.37 (m, 2H, pyrrole- β), 7.07 (s, 4H, *meso*-Mes), 6.94 (s, 2H, P-Mes), 2.47 (s, 6H, *meso-p*-Me), 2.33 (s, 3H, P-*p*-Me), 2.00 (s, 12H, *meso-o*-Me), 1.90 (br s, 6H, P-*o*-Me) ppm; ¹³C NMR (CDCl₃): δ 157.9 (d, $J = 12.2$ Hz), 148.5, 147.2 (d, $J = 26.5$ Hz), 142.1, 139.8, 137.9 (d, $J = 4.6$ Hz), 137.7, 135.0 (d, $J = 3.8$ Hz), 134.6 (d, $J = 10.3$ Hz), 132.1 (d, $J = 21.4$ Hz), 131.4 (d, $J = 15.8$ Hz), 129.6 (d, $J = 8.5$ Hz), 127.9, 127.8, 123.8 (d, $J = 38.4$ Hz), 119.7, 116.6, 22.4, 22.3, 21.4, 20.8 ppm; ³¹P NMR (CDCl₃): δ –42.0 ppm; HR-MS (ESI-MS): $m/z = 727.2473$, calcd for (C₄₅H₄₂N₄PNi)⁺ = 727.2495 [(M + H)⁺].

P-Mesityl-*meso*-mesityl-10-phosphacorrole oxide **2-O**.

A Schlenk tube containing 10-phosphacorrole Ni^{II} complex **2** (14.6 mg, 20.1 μ mol) was evacuated and then refilled with N₂. To the tube, dry and degassed CH₂Cl₂ (4.00 mL) was added. Then *m*CPBA (7.08 mg, 41.0 μ mol) was added to the tube and the mixture was stirred at r.t. for 5 minutes. The reaction mixture was extracted with CH₂Cl₂. The organic layer was washed with water, dried over anhydrous Na₂SO₄, and

concentrated in vacuo. Purification by silica-gel column chromatography with EtOAc afforded the title compound in 95% (14.2 mg, 19.1 μmol) as a blue solid. ^1H NMR (CDCl_3): δ 6.85 (s, 1H, P-Mes), 6.84 (s, 1H, P-Mes), 6.79 (s, 2H, *meso*-Mes), 6.78 (s, 2H, *meso*-Mes), 5.71 (dd, $J_1 = 4.5$ Hz, $J_2 = 2.5$ Hz, 2H, pyrrole- β), 5.61 (d, $J = 4.5$ Hz, 2H, pyrrole- β), 5.60 (dd, $J_1 = 4.5$ Hz, $J_2 = 2.5$ Hz, 2H, pyrrole- β), 5.56 (d, $J = 4.5$ Hz, 2H, pyrrole- β), 2.88 (s, 6H), 2.28 (s, 6H), 2.25–2.24 (m, 9H), 2.13 (s, 6H) ppm; ^{13}C NMR (CDCl_3): δ 158.5, 155.5, 154.6, 148.9, 145.5 (d, $J = 11.5$ Hz), 143.3, 143.1, 141.7 (d, $J = 2.4$ Hz), 139.4, 137.9, 136.2, 135.8, 132.9 (d, $J = 9.1$ Hz), 131.7, 131.5 (d, $J = 11.8$ Hz), 131.3, 128.0 (d, $J = 24.8$ Hz), 122.5 (d, $J = 19.3$ Hz), 118.2, 117.3, 116.3, 22.1, 22.0, 21.3, 21.1, 19.8, 19.7 ppm; ^{31}P NMR (CDCl_3): δ -14.0 ppm; HR-MS (ESI-MS): $m/z = 743.2419$, calcd for $(\text{C}_{45}\text{H}_{42}\text{N}_4\text{OPNi})^+ = 743.2442$ [(M + H) $^+$].

***P*-Mesityl-*meso*-mesityl-10-phosphacorrole Au^I complex 2-AuCl.**

A Schlenk tube containing 10-phosphacorrole Ni^{II} complex **2** (14.6 mg, 20.1 μmol) and chloro(dimethyl sulfide)gold(I) (12.1 mg, 41.1 μmol) was evacuated and then refilled with argon. To the tube, dry and degassed CH_2Cl_2 (7.00 mL) was added. The mixture was stirred at r.t. for 5 minutes. The reaction mixture was extracted with CH_2Cl_2 . The organic layer was washed with water, dried over anhydrous Na_2SO_4 , and concentrated in vacuo. Purification by silica-gel column chromatography with CH_2Cl_2 /hexane followed by recrystallization with CH_2Cl_2 /MeOH afforded the title compound in 68% (13.1 mg, 13.6 μmol) as a brown solid. ^1H NMR (CDCl_3): δ 7.01 (s, 2H, *meso*-Mes), 6.53–6.93 (m, 6H), 6.90 (s, 1H, P-Mes), 6.89 (s, 1H, P-Mes), 6.79 (d, $J = 4.5$ Hz, 2H, pyrrole- β), 6.20 (dd, $J_1 = 4.5$ Hz, $J_2 = 3.0$ Hz, 2H, pyrrole- β), 2.41–2.39 (m, 12H), 2.26 (s, 3H), 2.14 (s, 6H), 2.05 (s, 6H) ppm; ^{13}C NMR (CDCl_3): δ 154.0, 148.0, 147.4, 145.2 (d, $J = 11.0$ Hz), 143.4 (d, $J = 2.5$ Hz), 142.0, 141.1 (d, $J = 13.0$ Hz), 138.2, 137.7, 136.7 (d, $J = 22.8$ Hz), 133.1, 132.4 (d, $J = 9.6$ Hz), 131.9 (d, $J = 9.7$ Hz), 131.3, 128.3, 127.9, 123.6, 123.5, 117.7, 114.8, 114.3, 29.8, 24.0, 21.3, 21.2, 20.7, 20.4 ppm; ^{31}P NMR (CDCl_3): δ -22.9 ppm; HR-MS (ESI-MS): $m/z = 981.1677$, calcd for $(\text{C}_{45}\text{H}_{41}\text{N}_4\text{PNiAuClNa})^+ = 981.1669$ [(M + Na) $^+$].

NMR Spectra of Compounds

* = solvents and impurities

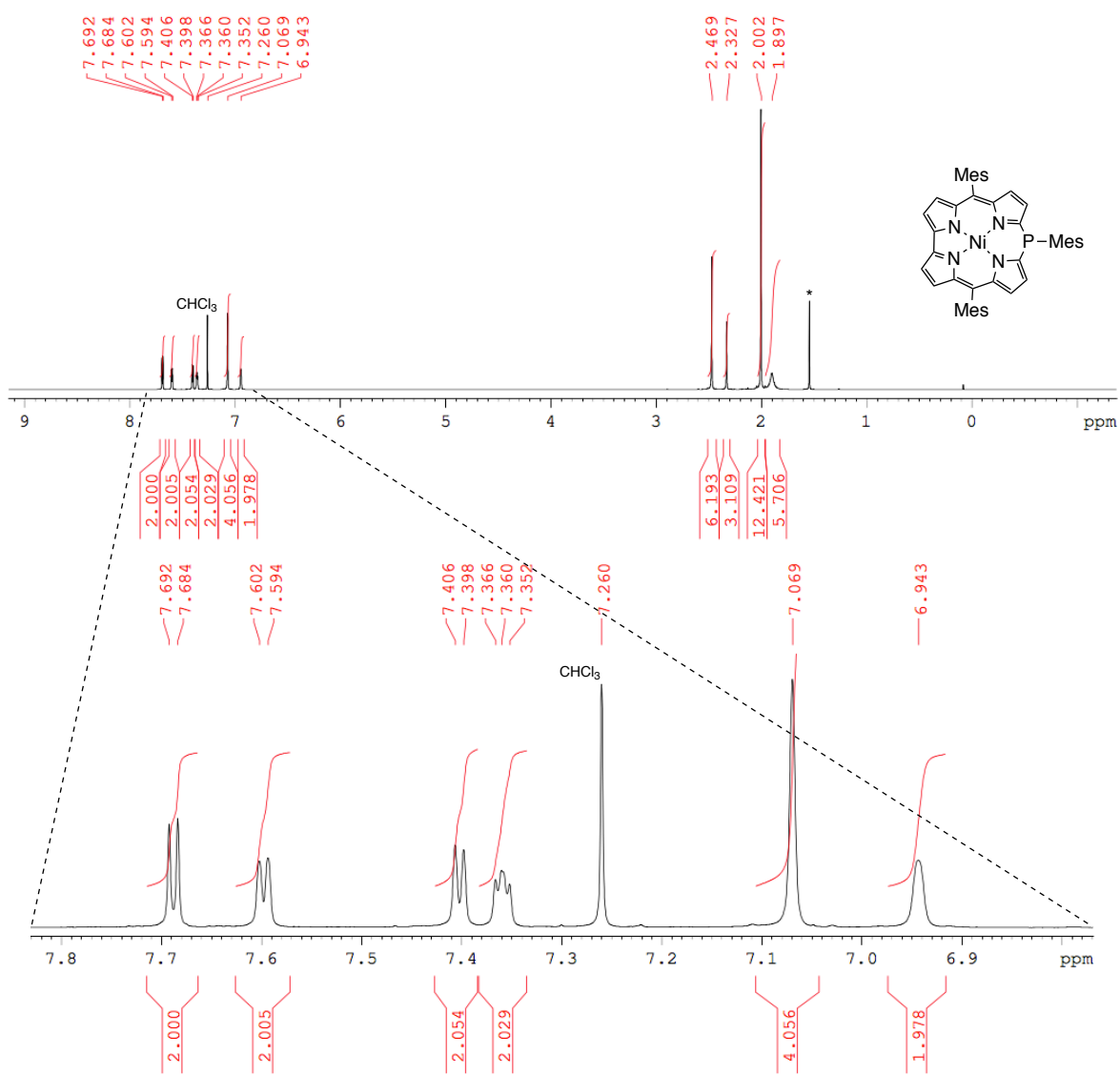


Figure S1. ¹H NMR spectrum of **2** in CDCl₃.

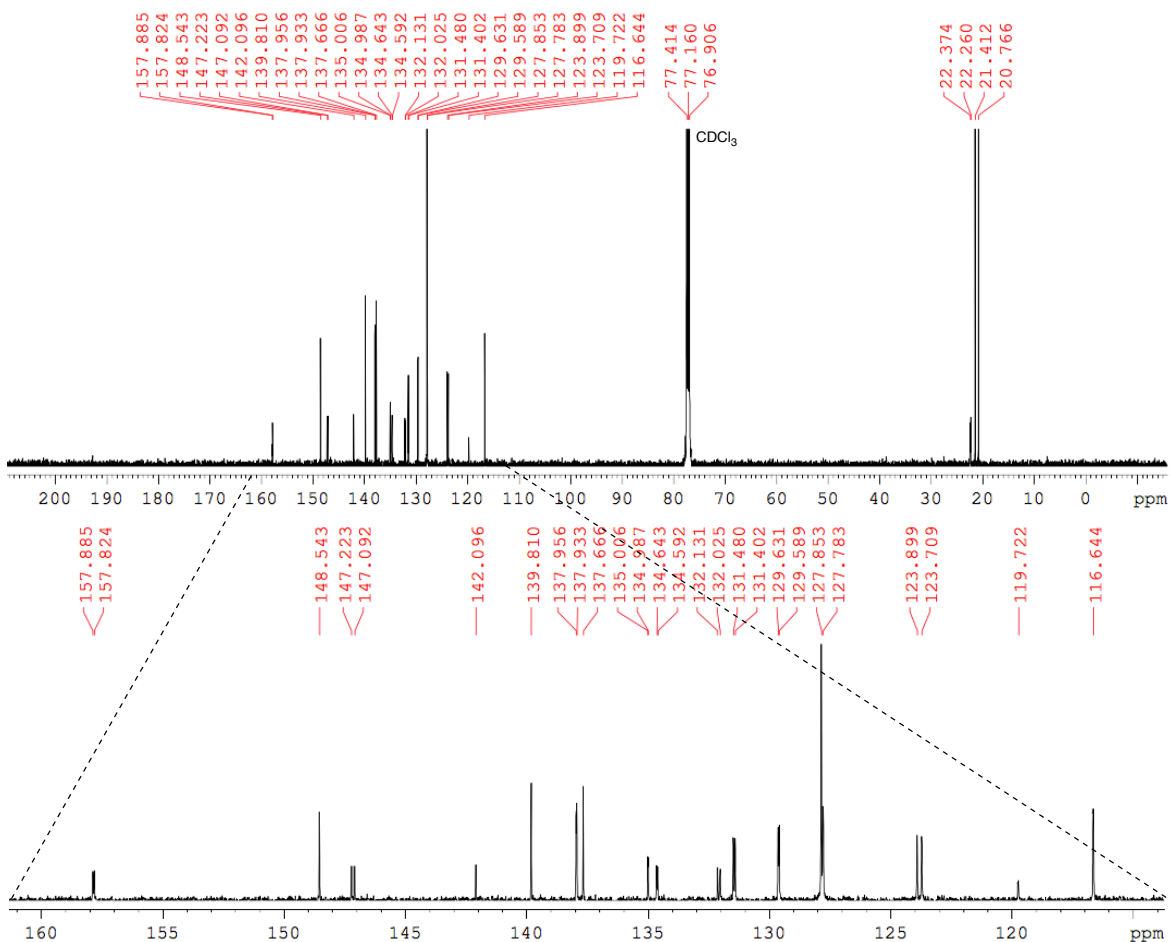


Figure S2. ^{13}C NMR spectrum of **2** in CDCl_3 .

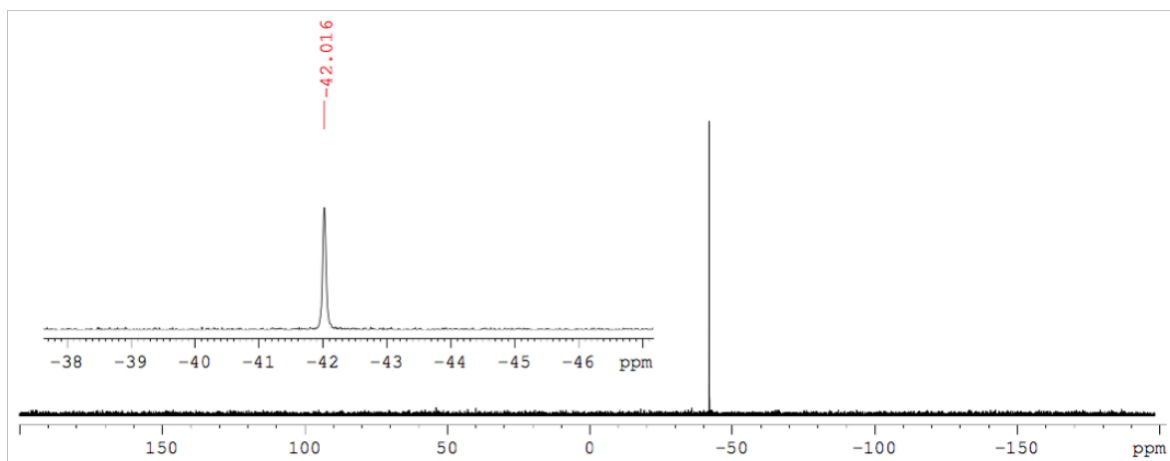


Figure S3. ^{31}P NMR spectrum of **2** in CDCl_3 .

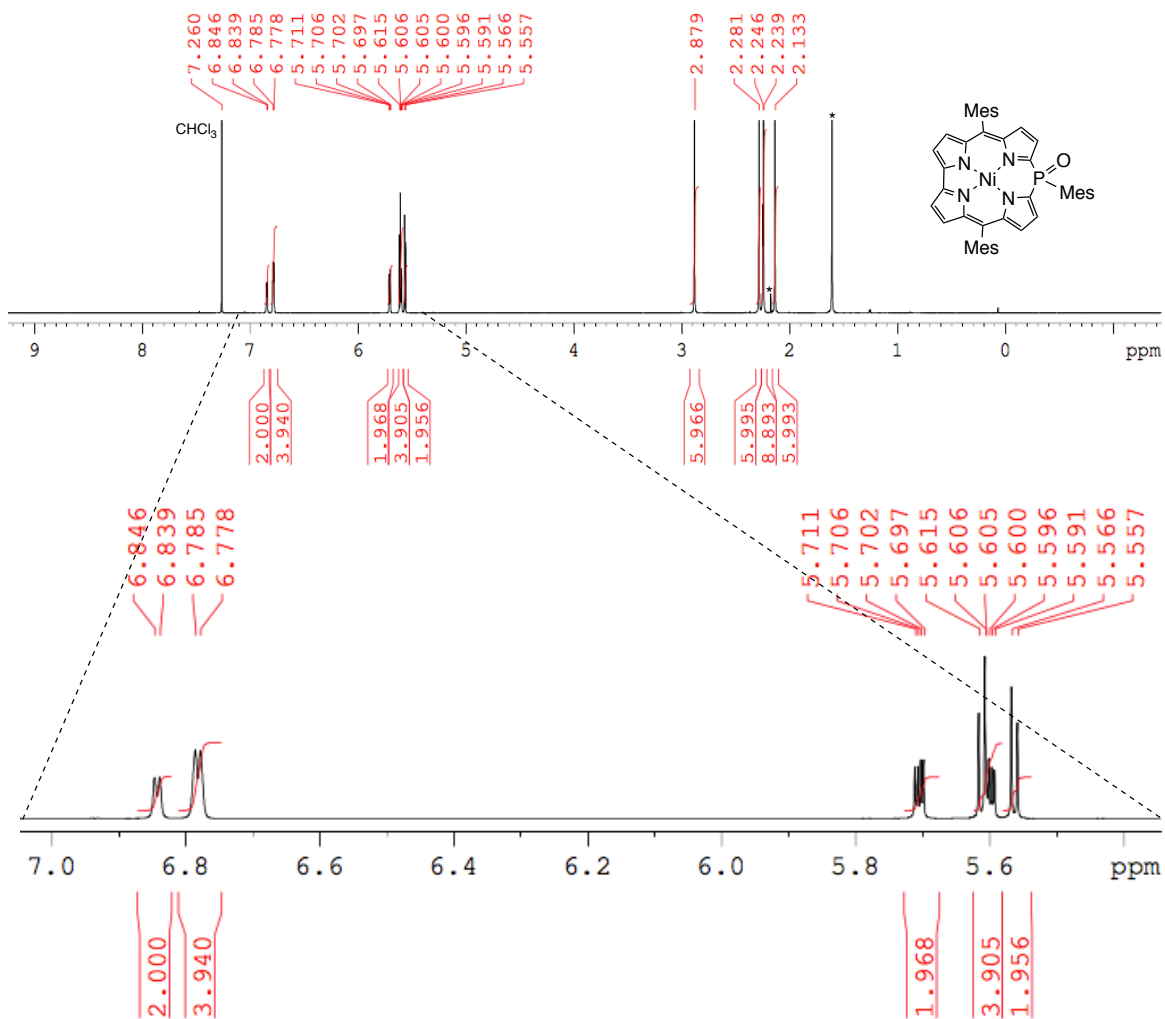


Figure S4. ^1H NMR spectrum of **2-O** in CDCl_3 .

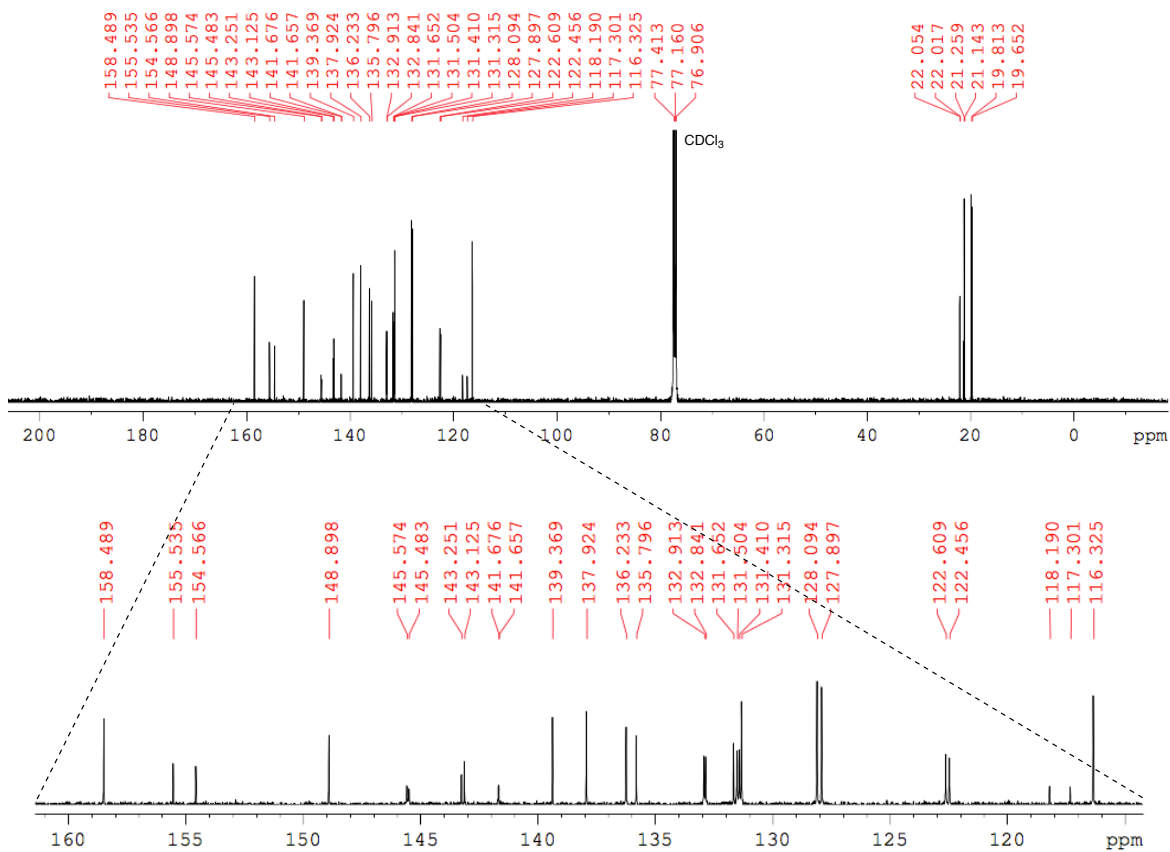


Figure S5. ^{13}C NMR spectrum of **2-O** in CDCl_3 .

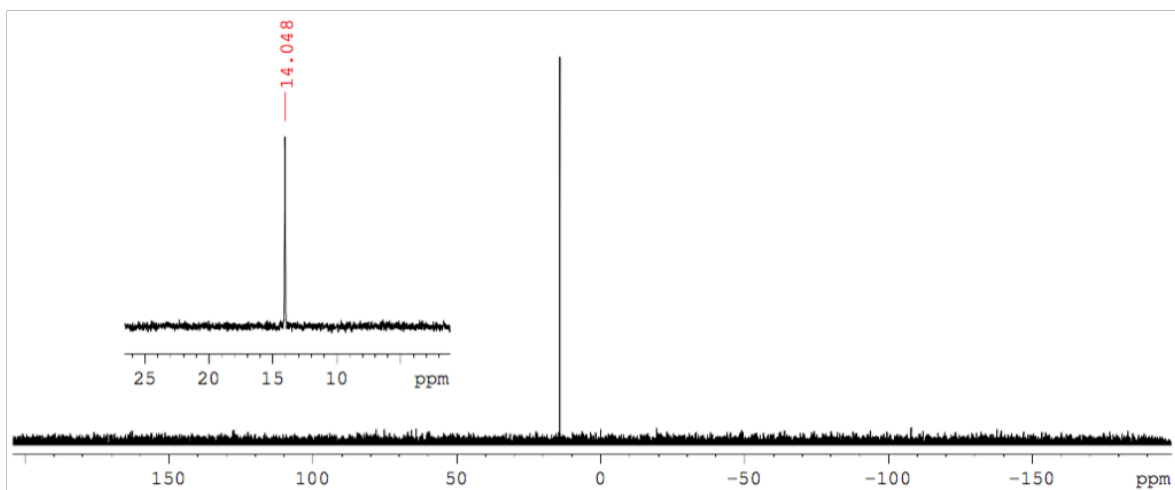


Figure S6. ^{31}P NMR spectrum of **2-O** in CDCl_3 .

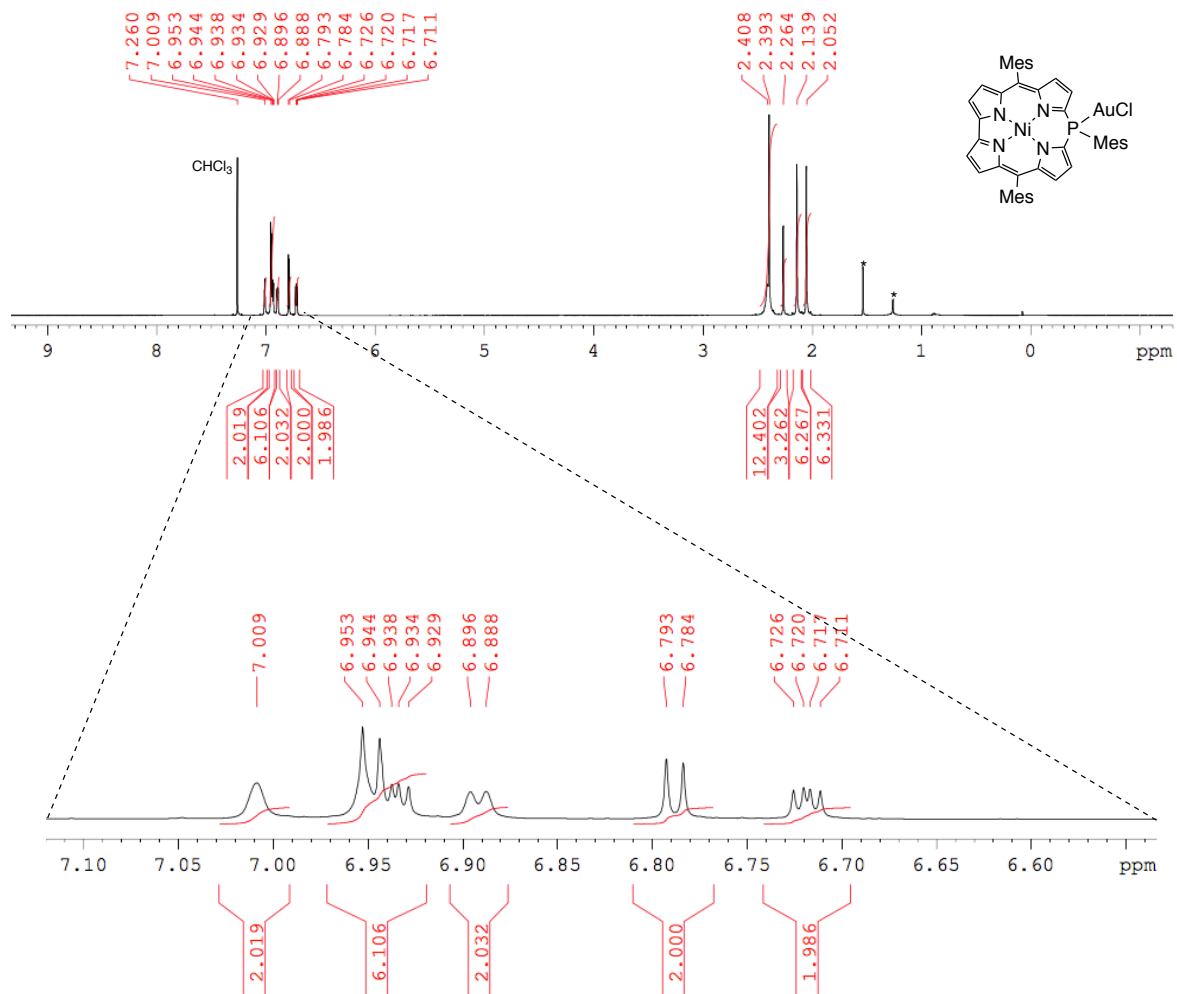


Figure S7. ^1H NMR spectrum of **2-AuCl** in CDCl_3 .

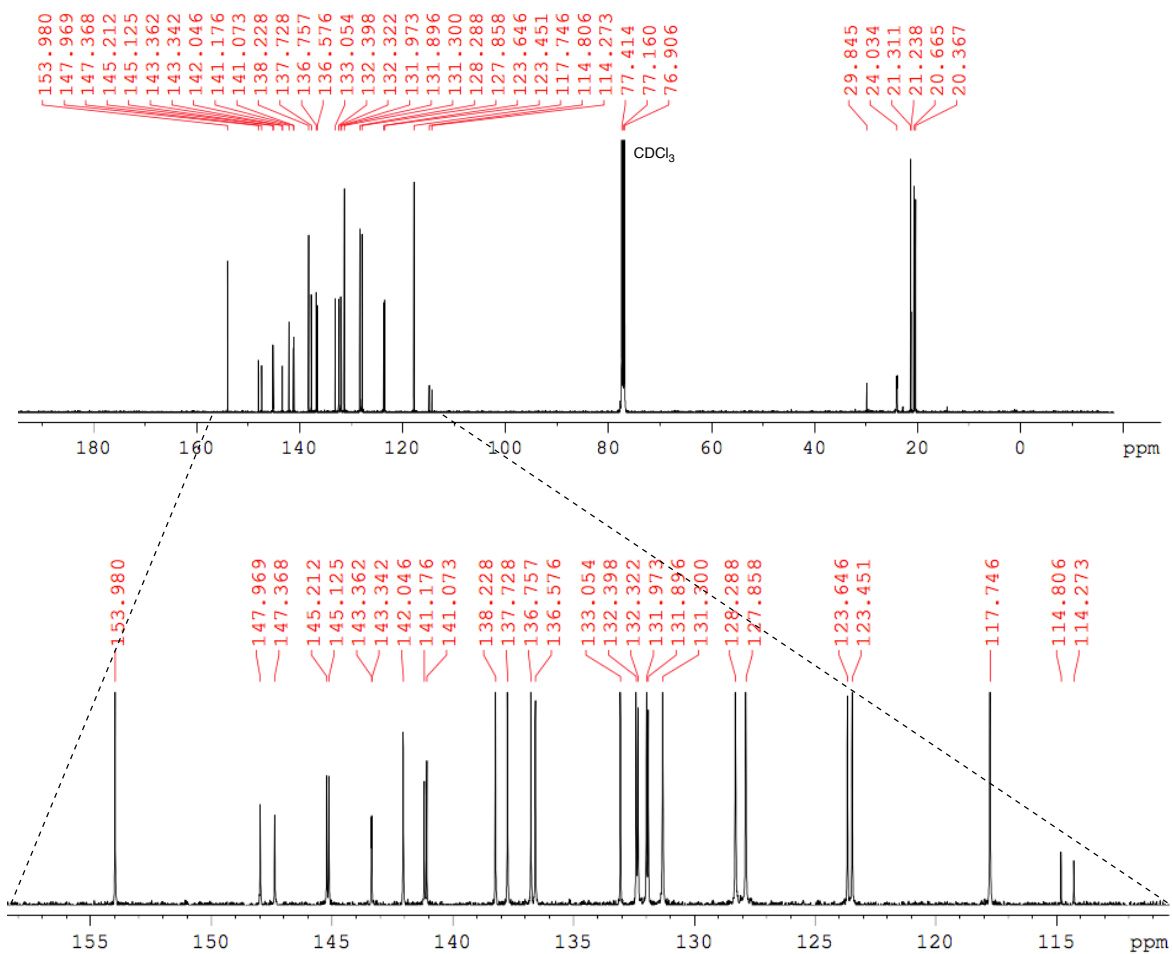


Figure S8. ^{13}C NMR spectrum of **2-AuCl** in CDCl_3 .

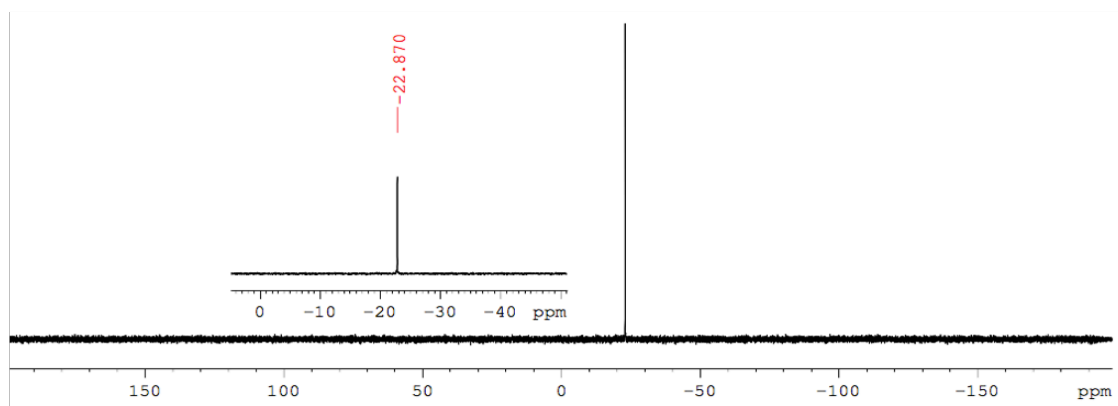


Figure S9. ^{31}P NMR spectrum of **2-AuCl** in CDCl_3 .

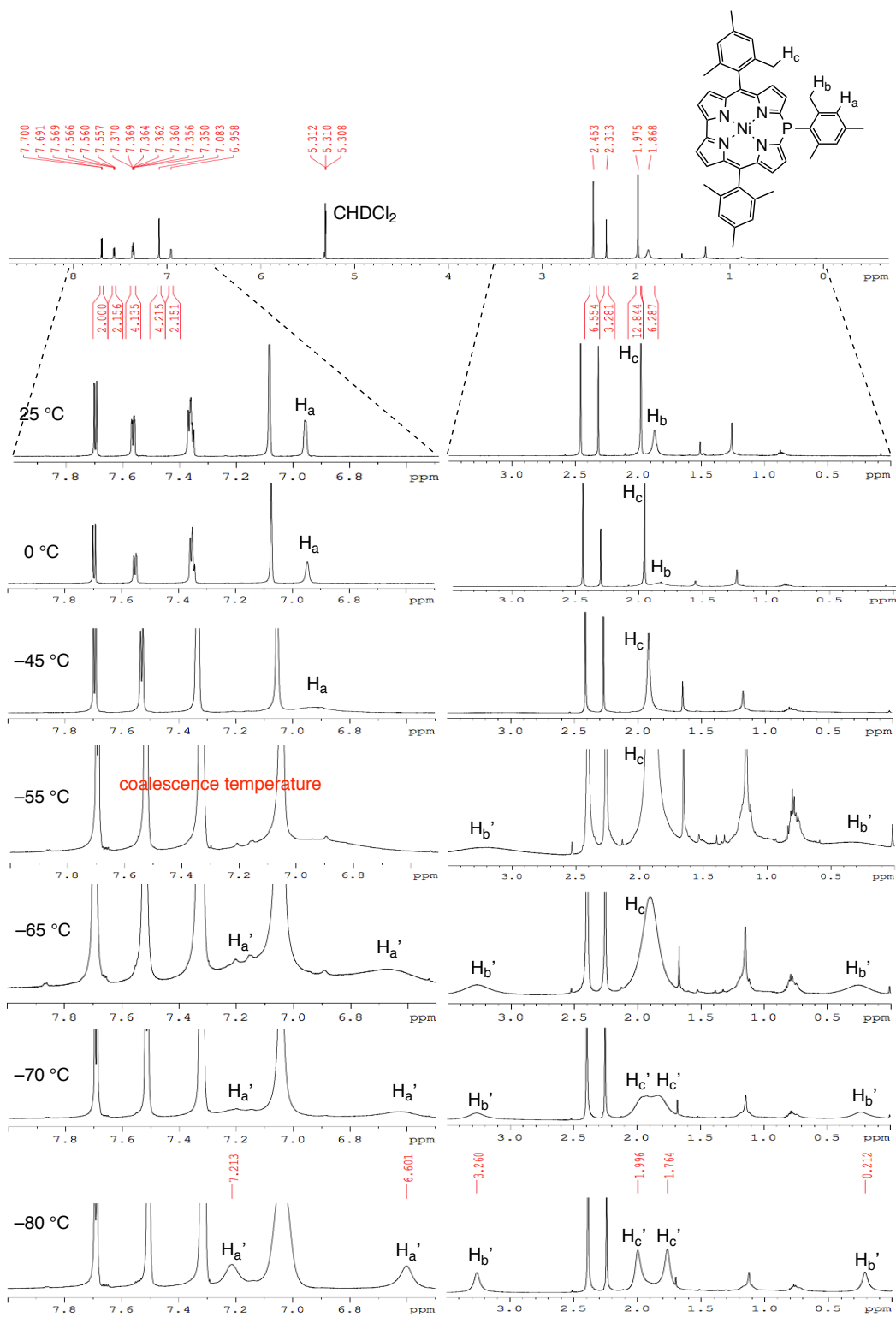


Figure S10. Temperature dependent ^1H NMR spectra of **2** in CD_2Cl_2 .

X-Ray Diffraction Analysis

X-ray crystallographic data of **2** and **2-AuCl** were obtained using a Bruker D8 QUEST X-ray diffractometer with an I μ S microfocuss X-ray source and a large area (10 cm \times 10 cm) CMOS detector (PHOTON 100). X-ray crystallographic data of **2-O** was taken on a Rigaku CCD diffractometer (Saturn 724 with MicroMax-007) with Varimax Mo optics using graphite monochromated Mo-K α radiation ($\lambda = 0.71075$ Å). Fine crystals of **2** for the X-ray diffraction analysis was obtained by the slow vapor diffusion of methanol into its chloroform solution. Fine crystals of **2-O** for the X-ray diffraction analysis was obtained by the slow vapor diffusion of octane into its toluene solution. Fine crystals of **2-AuCl** for the X-ray diffraction analysis was obtained by the slow vapor diffusion of methanol into its 1,2-dichloroethane solution. Crystallographic details are given in CIF files. Crystallographic data for **2**, **2-O**, and **2-AuCl** have been deposited with the Cambridge Crystallographic Data Centre as supplementary publication no. CCDC-1879940, 1879941, and 1879942, respectively.

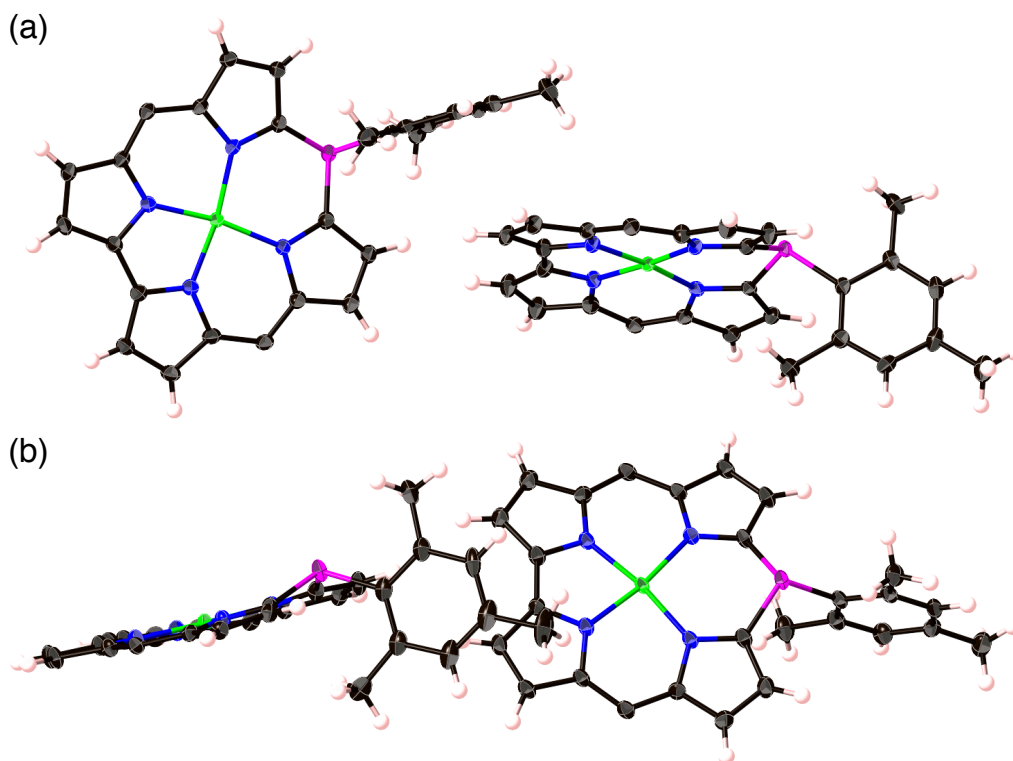


Figure S11. X-ray crystal structure of two independent molecules of **2**. (a) Top view and (b) side view. Thermal ellipsoids are scaled at 50% probability level. Mesityl groups are omitted for clarity.

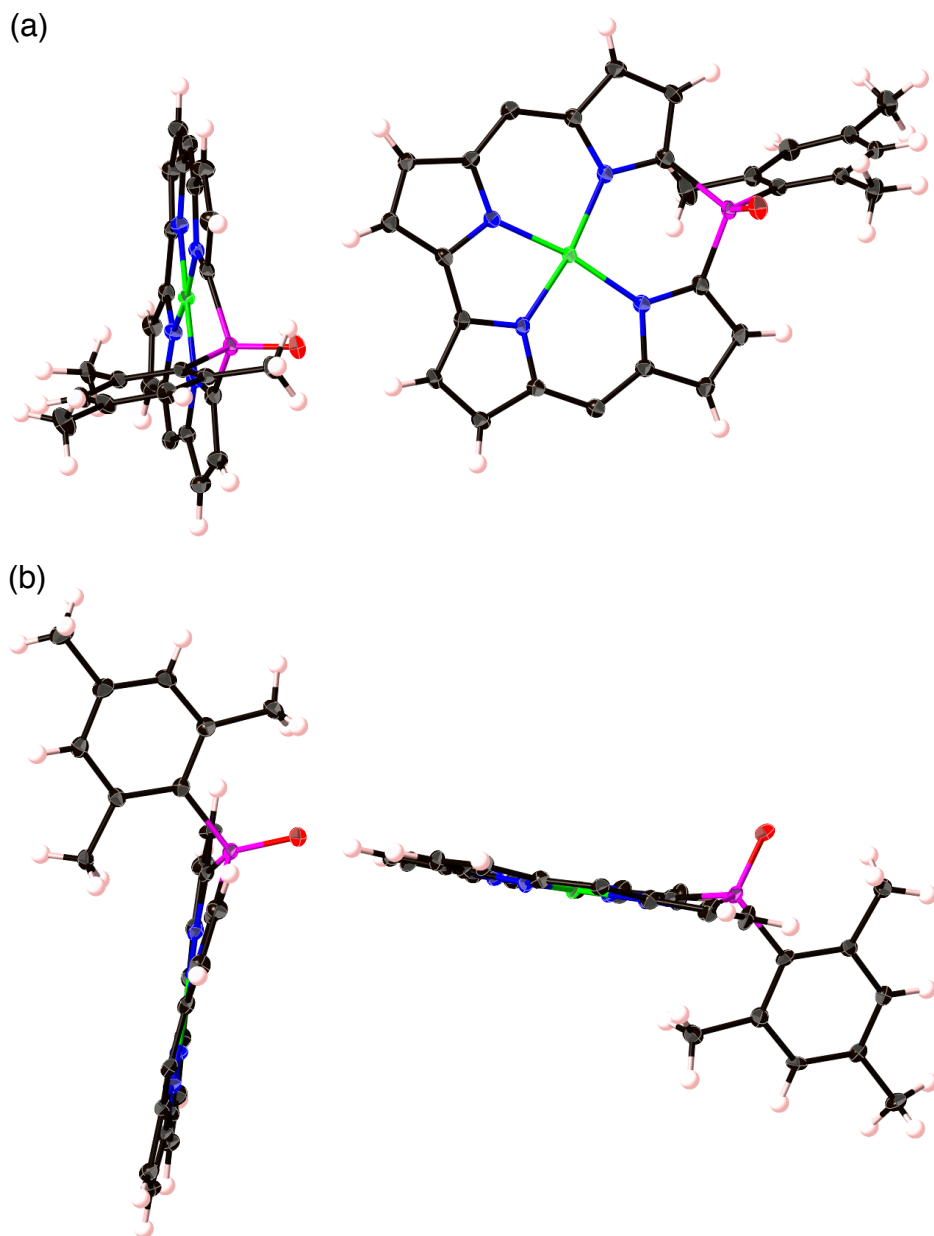


Figure S12. X-ray crystal structure of two independent molecules of **2-O**. (a) Top view and (b) side view. Thermal ellipsoids are scaled at 50% probability level. Mesityl groups are omitted for clarity.

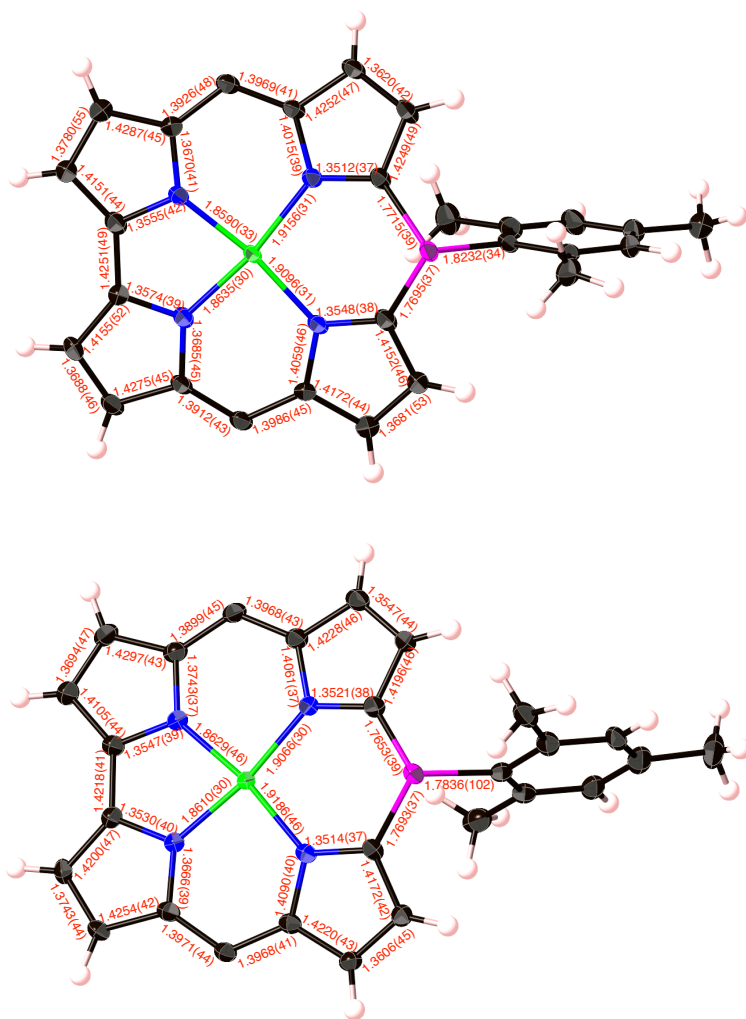


Figure S13. Selected bond lengths of **2**. Two individual molecules are shown.

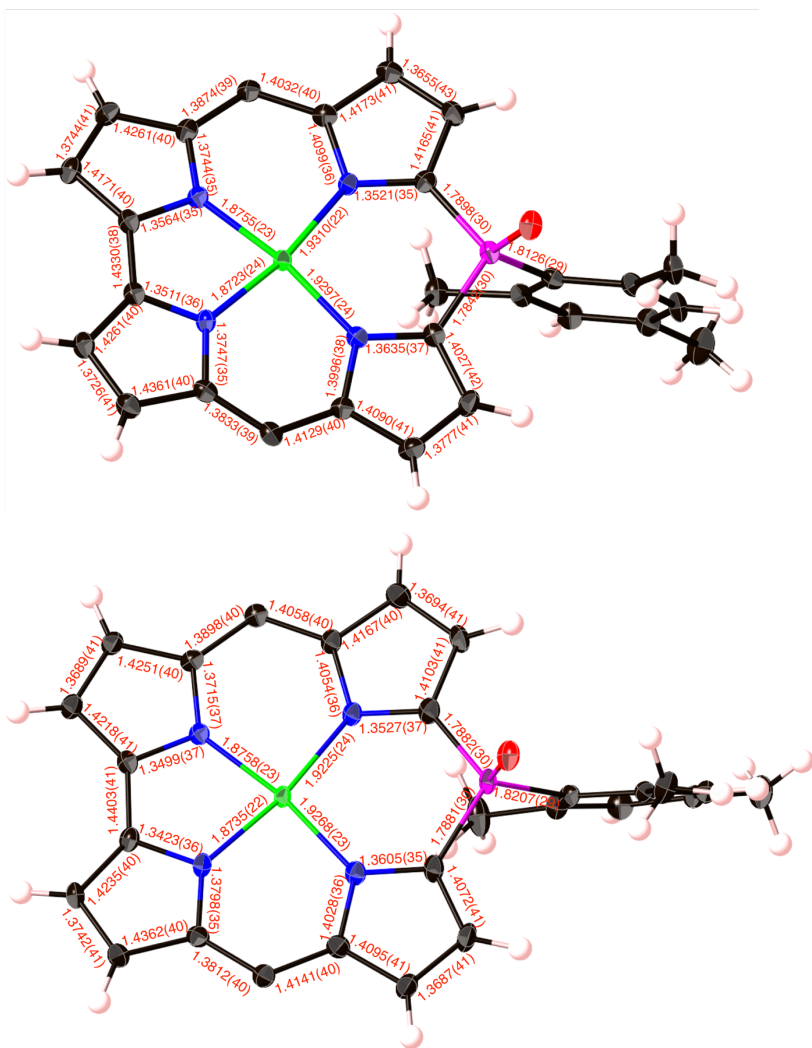


Figure S14. Selected bond lengths of 2-O. Two individual molecules are shown.

Table S1. Summary of X-ray crystallographic data of **2**, **2-O**, and **2-AuCl**.

	2	2-O	2-AuCl
empirical formula	C ₉₁ H ₈₃ N ₈ Ni ₂ P ₂ Cl ₃	C ₉₇ H ₉₀ N ₈ Ni ₂ O ₂ P ₂	C ₄₇ H ₄₅ N ₄ NiPAuCl ₃
moiety formula	2(C ₄₅ H ₄₁ N ₄ NiP), CHCl ₃	2(C ₄₅ H ₄₁ N ₄ NiOP), C ₇ H ₈	C ₄₅ H ₄₁ N ₄ NiPAuCl, C ₂ H ₄ Cl ₂
formula weight	1574.36	1579.12	1058.86
habit	prism	block	block
<i>T</i> , K	93(2)	107.(2)	113(2)
crystal system	triclinic	orthorhombic	triclinic
space group	<i>P</i> -1 (2)	<i>Pbca</i> (61)	<i>P</i> -1 (2)
<i>a</i> , Å	16.0007(10)	16.4476(3)	12.7696(6)
<i>b</i> , Å	16.1997(10)	24.3351(4)	13.2248(6)
<i>c</i> , Å	17.7476(12)	40.0869(5)	15.5398(7)
<i>α</i> , deg	100.329(2)	90	98.6560(10)
<i>β</i> , deg	115.508(2)	90	107.3330(10)
<i>γ</i> , deg	101.094(2)	90	113.7310(10)
<i>V</i> , Å ³	3891.7(4)	16044.9(4)	2180.75(17)
<i>Z</i>	2	8	2
<i>D_c</i> , g/cm ³	1.344	1.307	1.613
<i>F</i> (000)	1644	6640	1056
crystal size, mm ³	0.50 x 0.38 x 0.31	0.44 x 0.43 x 0.30	0.46 x 0.17 x 0.050
2 θ_{\max} , °	50.2	50.0	50.1
<i>R</i> ₁ (<i>I</i> > 2 σ (<i>I</i>))	0.0428	0.0457	0.0202
<i>wR</i> ₂ (all data)	0.1216	0.1380	0.0559
GOF	1.075	1.093	1.048
obs reflects	11824	11073	7180
total reflects	13132	14126	7349
parameters	1095	1019	560

Electrochemical Analysis

The cyclic voltammogram and differential-pulse voltammogram of **2**, **2-O**, and **2-AuCl** were recorded using an ALS electrochemical analyzer 612C. Measurements were performed in freshly distilled CH_2Cl_2 with tetrabutylammonium hexafluorophosphate as the electrolyte. A three-electrode system was used. The system consisted of a platinum working electrode, a platinum wire, and Ag/AgClO_4 as the reference electrode. The scan rate was 100 mVs^{-1} . The measurement was performed under nitrogen atmosphere. All potentials are referenced to the potential of ferrocene/ferrocenium cation couple.

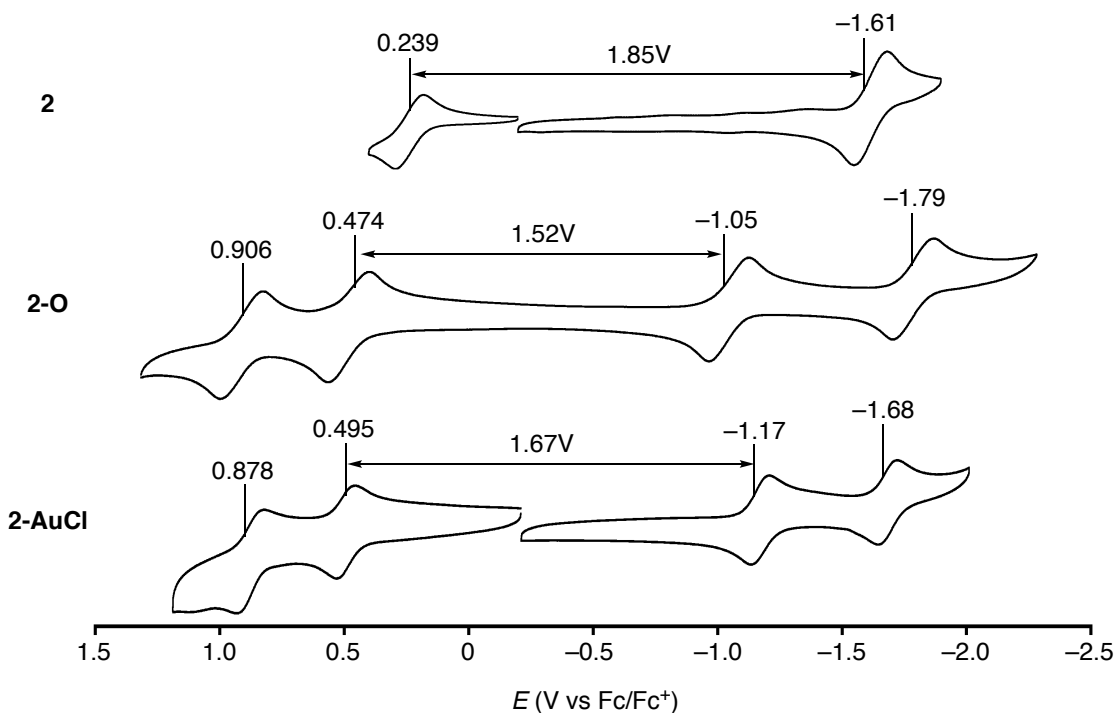


Figure S16. Cyclic voltammograms of **2**, **2-O**, and **2-AuCl** in CH_2Cl_2 .

Theoretical Calculations

All calculations were carried out using the *Gaussian 09* program.² Geometries of azacorrole, **2**, and **2-O** were obtained from their X-ray structures but the mesityl substituents at the meso-position were replaced with hydrogen atom to reduce the calculation cost. All the structures were fully optimized without any symmetry restriction at the Becke's three-parameter hybrid exchange functional and the Lee–Yang–Parr correlation functional (B3LYP)³ and a basis set consisting of SDD⁴ for Ni and 6-31G(d) for the rest. For the calculation of the inversion energy of the phosphorus center in **2**, a rough transition state geometry was obtained using the *Reaction plus Pro* software package,⁵ based on the nudged elastic band (NEB) method.⁶ Then the transition state geometry was fully optimized at the B3LYP/6-31G(d)+SDD level. The transition state gave single imaginary frequency and the IRC calculation also supported the structure. Zero-point energy and thermal energy corrections were conducted at the B3LYP/6-31G(d)+SDD level, and the sums of electronic and thermal free energies were obtained. The zero-point energies were not scaled, and the enthalpic corrections were made at 218.15 K. The energies of the ground and transition states were further obtained by the single point calculation at the B3LYP/6-311+G(2d,p)+SDD.

The NICS DFT calculations were performed using gaug-including atomic orbitals (GIAOs) at the B3LYP/6-31G(d)+SDD level. For the NICS calculations of the hypothetical free base 10-phosphacorrole and its derivatives, the Ni atom in each molecule was replaced with two hydrogen atoms. The ACID calculation was performed at the CGST-B3LYP/def2-TZVP level. NBO analyses were conducted at the B3LYP/def2-TZVP level.

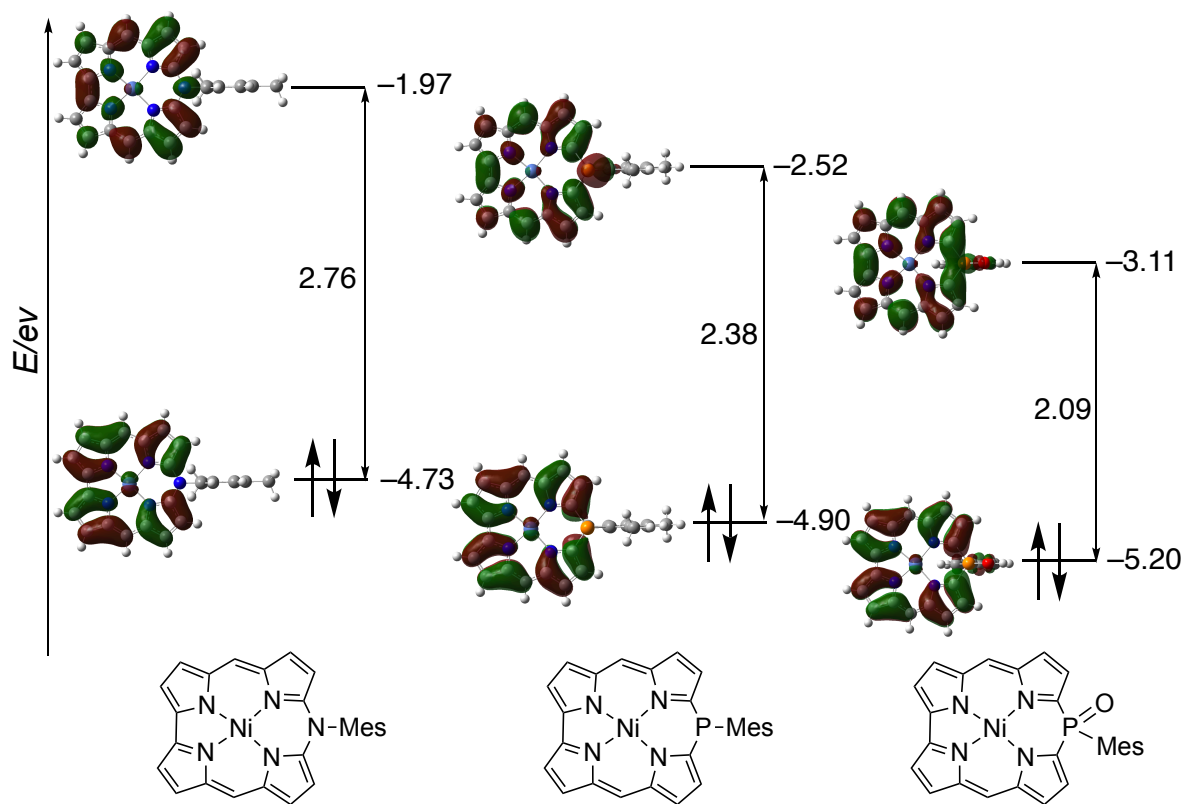


Figure S17. MO diagrams of 10-azacorrole, 10-phosphaorrole, and 10-phoshaorrole oxide at the B3LYP/6-31G(d)+SDD level.

Table S2. Interaction energies of interacting donor–acceptor NBOs in **2-O** and **2-AuCl**.

Compound	Donor NBO	Acceptor NBO	Energy (kcal mol ⁻¹)
2-O	π C=N (NBO 68)	σ^* P–O (NBO 134)	1.88
	π C=N (NBO 68)	σ^* P–C (NBO 136)	1.18
	π C=N (NBO 71)	σ^* P–O (NBO 134)	1.89
	π C=N (NBO 71)	σ^* P–C (NBO 136)	1.15
2-AuCl	σ P–Au (NBO 145)	π^* C=N (NBO 170)	8.65
	σ P–Au (NBO 145)	π^* C=N (NBO 174)	8.51

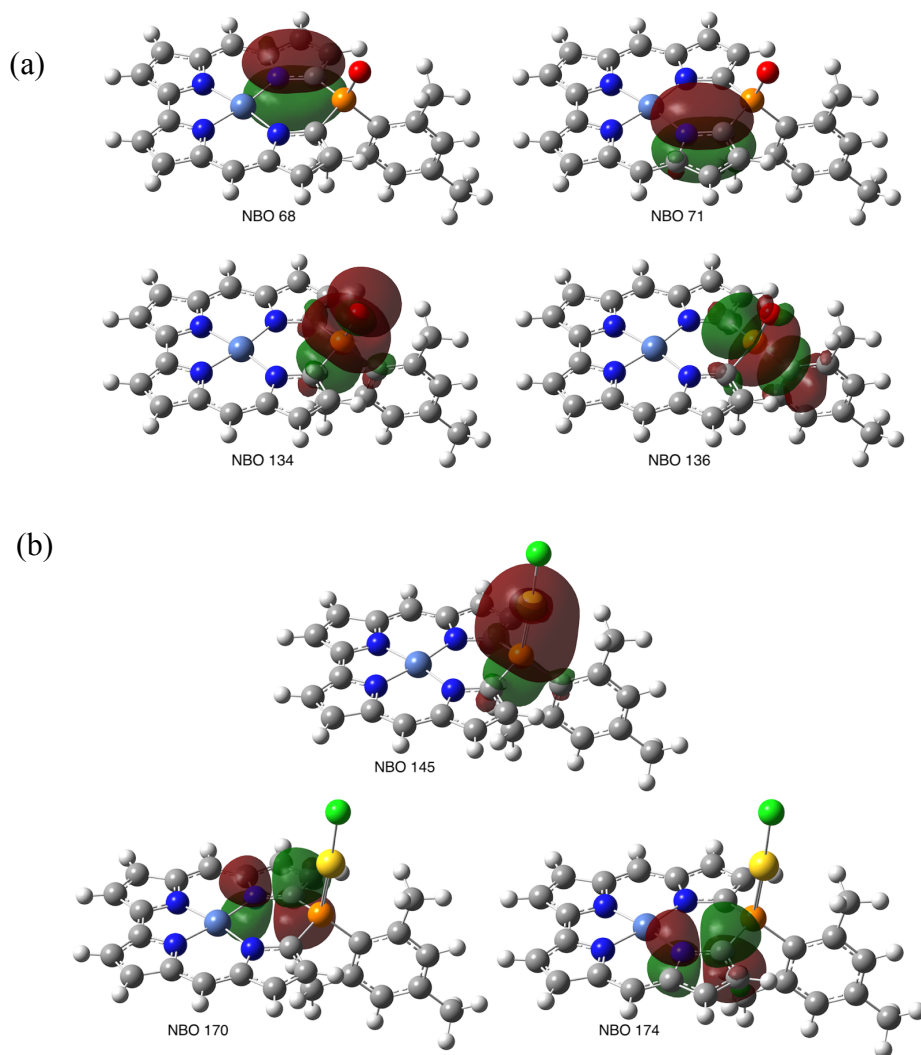


Figure S18. Selected NBOs of (a) **2-O** and (b) **2-AuCl**.

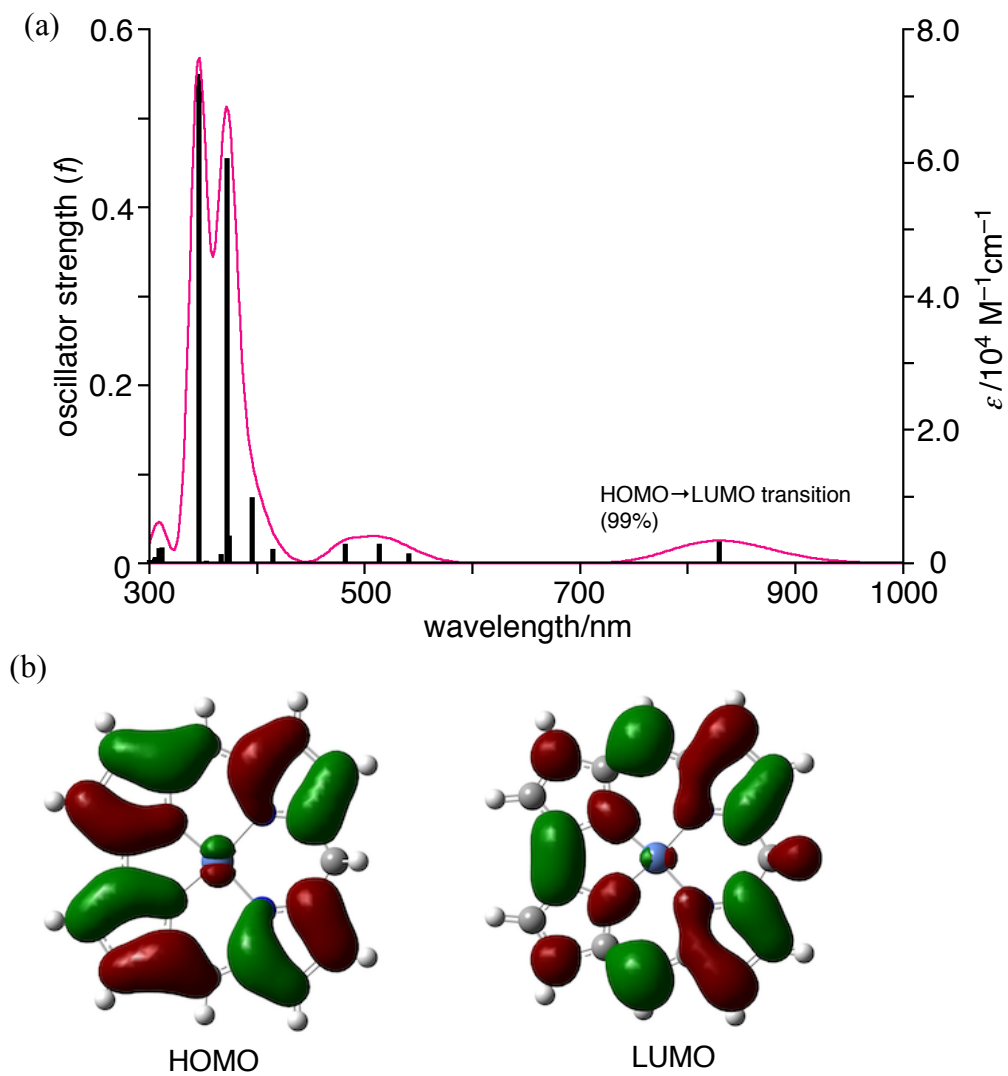


Figure S19. (a) Simulated absorption spectra of **2-O** and (b) HOMO and LUMO of Ni(II) isocorrole calculated at the B3LYP/6-31G(d)+SDD level. The calculated spectral curve was obtained with a half-band width of 800 cm^{-1} using *GaussView 6.0* program.

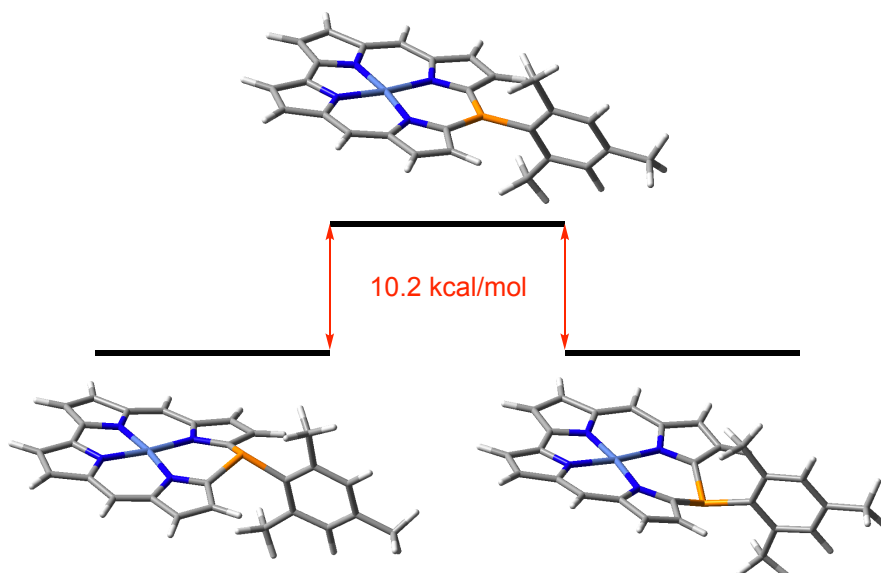


Figure S20. Energy profile for pyramidal inversion of **2** by DFT calculations. The geometries were optimized at the B3LYP/6-31G(d)+SDD level. The energy was obtained at the B3LYP/6-311+G(2d,p)+SDD level.

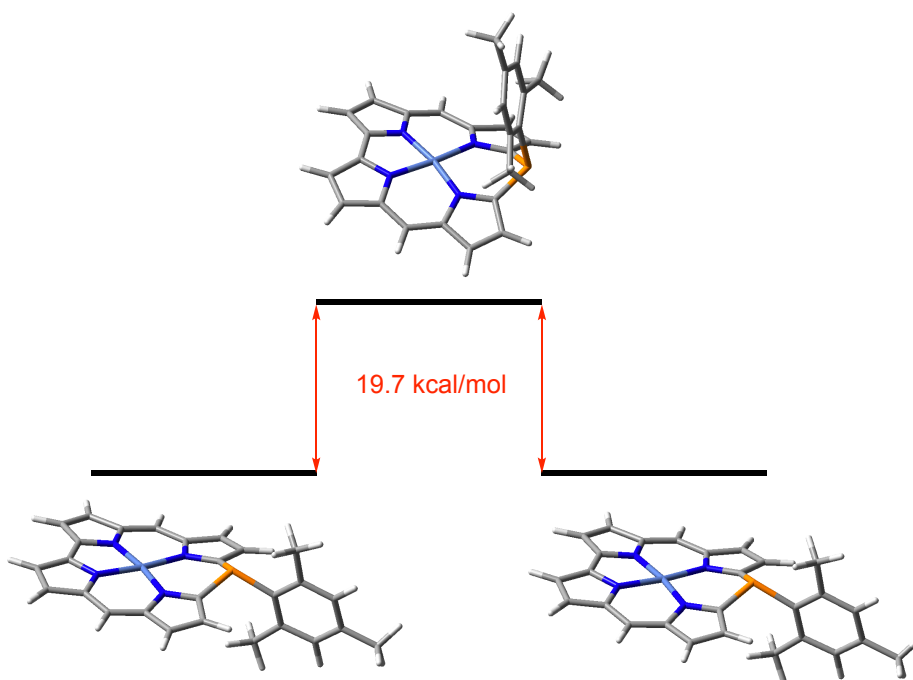


Figure S21. Energy profile for rotation of the mesityl group on phosphorus of **2** by DFT calculations. The geometries were optimized at the B3LYP/6-31G(d)+SDD level. The energy was obtained at the B3LYP/6-311+G(2d,p)+SDD level.

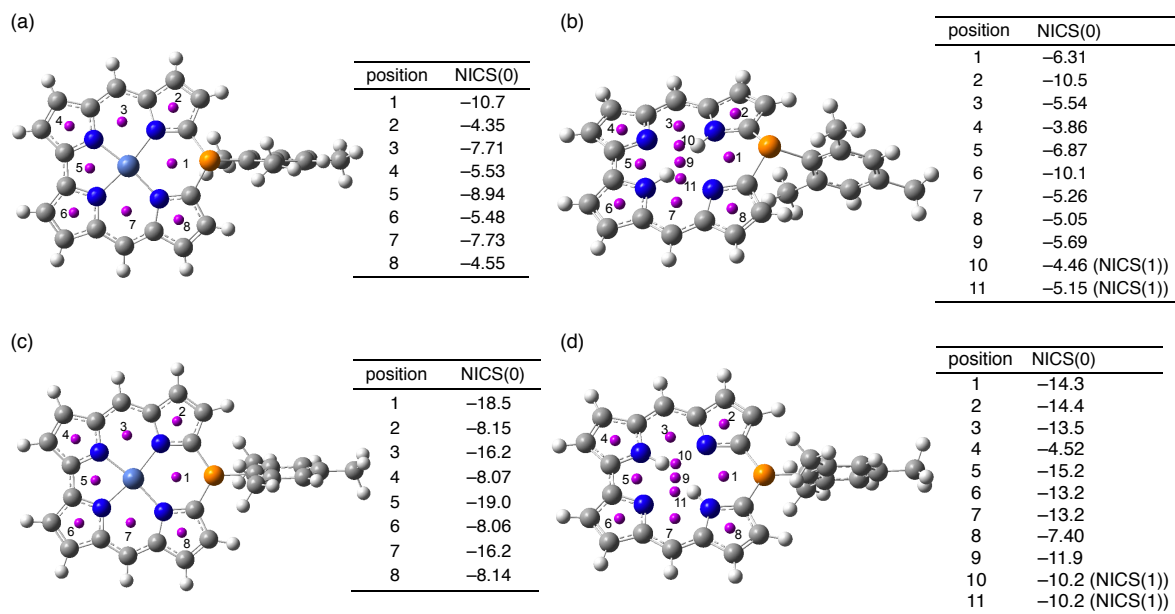


Figure S22. NICS values of **2** (B3LYP/6-31G(d)+SDD level) and its hypothetical free-base 10-phosphacorrole (B3LYP/6-31G(d) level). (a) and (b) the pyramidal ground state and (c) and (d) the planar transition state.

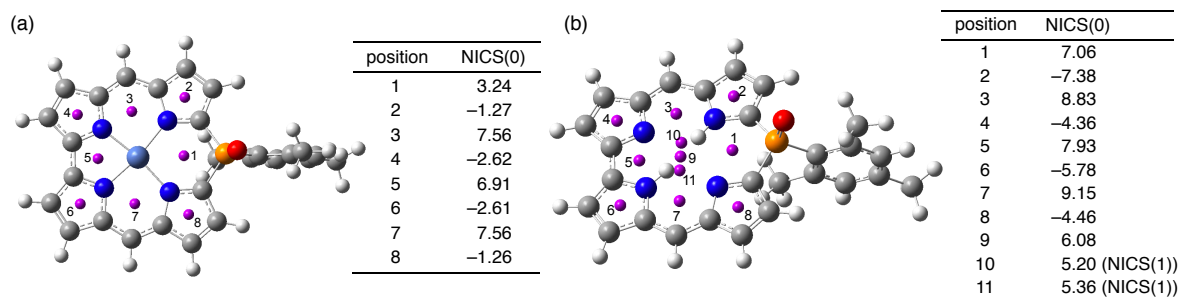


Figure S23. NICS values of (a) **2-O** (B3LYP/6-31G(d)+SDD level) and (b) its hypothetical free-base 10-phosphacorrole oxide (B3LYP/6-31G(d) level).

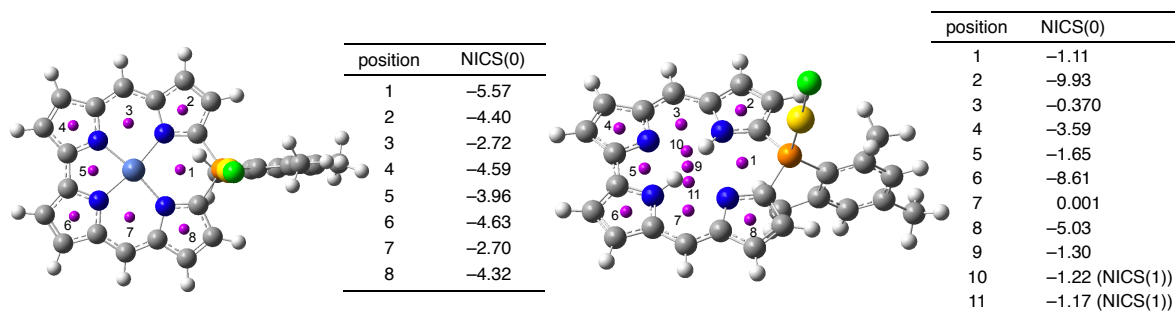


Figure S24. NICS values of (a) **2-AuCl** (B3LYP/6-31G(d)+SDD level) and (b) its hypothetical free-base 10-phosphacorrole AuCl complex (B3LYP/6-31G(d)+SDD level).

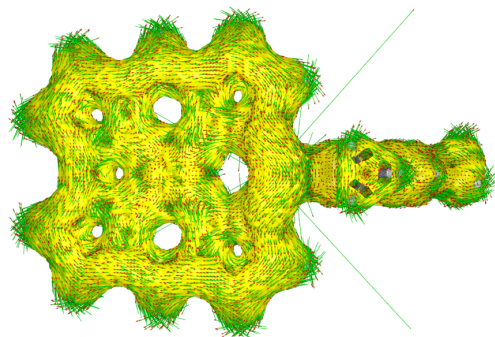


Figure S25. ACID plots of **2** (isovalue 0.02) calculated at the CSGT-B3LYP/def2-TZVP level.

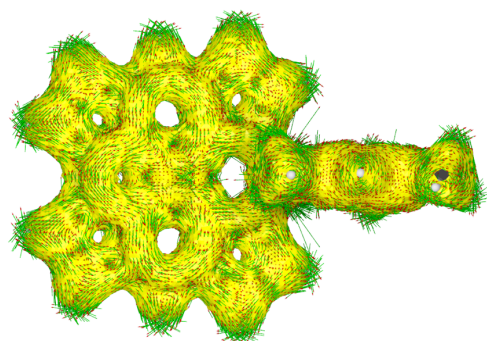


Figure S26. ACID plots of **2-O** (isovalue 0.02) calculated at the CSGT-B3LYP/def2-TZVP level.

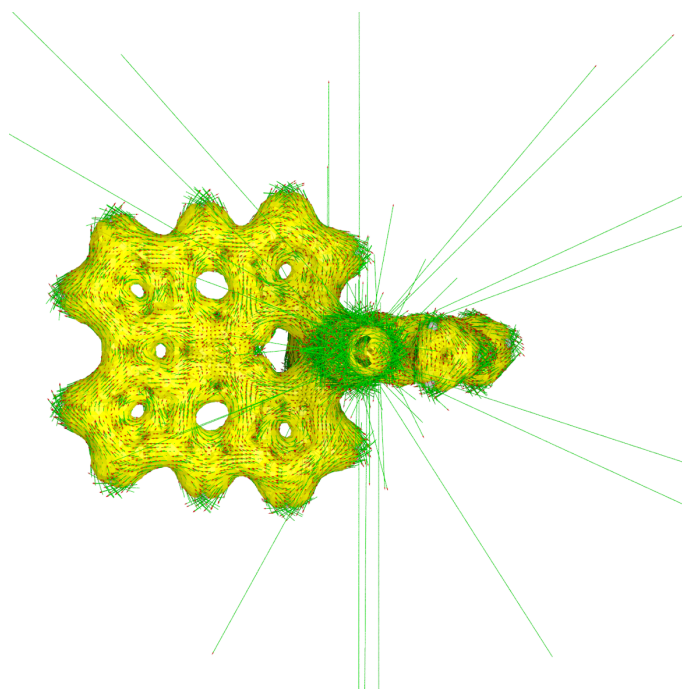


Figure S27. ACID plots of **2-AuCl** (isovalue 0.02) calculated at the CSGT-B3LYP/def2-TZVP level.

GIMIC Calculation

The GIMIC calculations were based on the optimized geometries of **2**, **2-O**, and **2-AuCl**, which are obtained with the B3LYP functional and the Karlsruhe def2-TZVP basis sets starting from their X-ray structures. Relativistic effects have been treated by using extended core potentials for Au.⁷ Dispersion effects have been taken into account by using the Becke-Johnson damped D3 correction.⁸ The mesityl groups at the *meso*-carbon atoms have been replaced by hydrogen for obtaining a clearer picture of the current density pattern. Nuclear magnetic shieldings were calculated with Turbomole 7.3⁹ using the BHLYP¹⁰ functional together with the Karlsruhe def2-TZVP basis sets.¹¹ Magnetically induced current densities were calculated on the same level of theory using the GIMIC program,¹² which is a free available open-source program. The molecules have been oriented in the xy plane and the external magnetic field has been placed in z-direction. GIMIC uses the atomic orbital density matrix, the first-order magnetically perturbed density matrices and basis-set information as input data. The density matrices are obtained from nuclear magnetic shielding calculations in the present case on BHLYP/def2-TZVP level. Gauge origin independence and a fast basis-set convergence are assured in the current-density calculations, because gauge-including atomic orbitals (GIAOs) are employed.¹³ Integrated current strength susceptibilities and current pathways were obtained by performing numerical integration of the current flow passing through chemical bonds of interest. The integrated current strength susceptibility is given in nA T⁻¹.

References

- 1) Matano, Y.; Shibano, T.; Nakano, H.; Imahori, H. *Chem. Eur. J.* **2012**, *18*, 6208.
- 2) Gaussian 09, Revision D.01, Frisch, M. J.; Trucks, G. W.; Schlegel, H. B.; Scuseria, G. E.; Robb, M. A.; Cheeseman, J. R.; Scalmani, G.; Barone, V.; Mennucci, B.; Petersson, G. A.; Nakatsuji, H.; Caricato, M.; Li, X.; Hratchian, H. P.; Izmaylov, A. F.; Bloino, J.; Zheng, G.; Sonnenberg, J. L.; Hada, M.; Ehara, M.; Toyota, K.; Fukuda, R.; Hasegawa, J.; Ishida, M.; Nakajima, T.; Honda, Y.; Kitao, O.; Nakai, H.; Vreven, T.; Montgomery, Jr., J. A.; Peralta, J. E.; Ogliaro, F.; Bearpark, M.; Heyd, J. J.; Brothers, E.; Kudin, K. N.; Staroverov, V. N.; Kobayashi, R.; Normand, J.; Raghavachari, K.; Rendell, A.; Burant, J. C.; Iyengar, S. S.; Tomasi, J.; Cossi, M.; Rega, N.; Millam, J. M.; Klene, M.; Knox, J. E.; Cross, J. B.; Bakken, V.; Adamo, C.; Jaramillo, J.; Gomperts, R.; Stratmann, R. E.; Yazyev, O.; Austin, A. J.; Cammi, R.; Pomelli, C.; Ochterski, J. W.; Martin, R. L.; Morokuma, K.; Zakrzewski, V. G.; Voth, G. A.; Salvador, P.;

- Dannenberg, J. J.; Dapprich, S.; Daniels, A. D.; Farkas, Ö.; Foresman, J. B.; Ortiz, J. V.; Cioslowski, J.; Fox, D. J. Gaussian, Inc., Wallingford CT, 2009.
- 3) (a) Becke, A. D. *Phys. Rev. A* **1988**, *38*, 3098. (b) Lee, C.; Yang, W.; Parr, R. G. *Phys. Rev. B* **1988**, *37*, 785.
 - 4) Dolg, M.; Wedig, U.; Stoll, H.; Preuss, H. *J. Chem. Phys.* **1987**, *86*, 866.
 - 5) Software to optimize reaction paths along the user's expected ones, HPC Systems Inc., <http://www.hpc.co.jp/chem/react1.html>.
 - 6) (a) Jónsson, H.; Mills, G.; Jacobsen, K. W. in *Classical and Quantum Dynamics in Condensed Phase Simulations*, (Eds.: B. J. Berne, G. Ciccotti, D. F. Coker), World Scientific Publishing, **1998**, p. 385. (b) Henkelman, G.; Jónsson, H. *J. Chem. Phys.* **2000**, *113*, 9978.
 - 7) Andrae, D.; Haeussermann, U.; Dolg, M.; Stoll, H.; Preuss, H. *Theor. Chim. Acta* **1990**, *77*, 123.
 - 8) (a) Grimme, S.; Ehrlich, S.; Goerigk, L. *J. Comp. Chem.* **2011**, *32*, 1456. (b) Grimme, S.; Antony, J.; Ehrlich, S.; Krieg, H. *J. Chem. Phys.* **2010**, *132*, 154104.
 - 9) (a) Ahlrichs, R.; Bär, M.; Häser, M.; Hornand, H.; Kölmel, C. *Chem. Phys. Lett.* **1989**, *162*, 165. (b) Furche, F.; Ahlrichs, R.; Hättig, C.; Klopper, W.; Sierka, M.; Weigend, F. *WIREs. Comput. Mol. Sci.* **2014**, *4*, 91.
 - 10) Becke, A. D. *J. Chem. Phys.* **1993**, *98*, 1372
 - 11) (a) Schäfer, A.; Horn, H.; Ahlrichs, R. *J. Chem. Phys.* **1992**, *97*, 2571. (b) Weigend, F.; Ahlrichs, R. *Phys. Chem. Chem. Phys.* **2005**, *7*, 3297. (c) Eichkorn, K.; Weigend, F.; Treutler, O.; Ahlrichs, R. *Theor. Chem. Acc.* **1997**, *97*, 119.
 - 12) (a) Jusélius, J.; Sundholm, D.; Gauss, J. *J. Chem. Phys.* **2004**, *121*, 3952. (b) Taubert, S.; Sundholm, D.; Jusélius, J. *J. Chem. Phys.* **2011**, *134*, 054123. (c) Fliegl, H.; Taubert, S.; Lehtonen, O.; Sundholm, D. *Phys. Chem. Chem. Phys.* **2011**, *13*, 20500.
 - 13) (a) Ditchfield, R. *Mol. Phys.* 1974, *27*, 789. (b) Wolinski, K.; Hinton, J. F.; Pulay, P. *J. Am. Chem. Soc.* **1990**, *112*, 8251.